SEARCH FOR RESONANT DOUBLE HIGGS PRODUCTION WITH BBZZ DECAYS IN THE $b\bar{b}\ell\ell\nu\bar{\nu}$ FINAL STATE IN pp COLLISIONS AT $\sqrt{s} = 13$ TeV

by

Rami Kamalieddin

A DISSERTATION

Presented to the Faculty of

The Graduate College at the University of Nebraska

In Partial Fulfilment of Requirements

For the Degree of Doctor of Philosophy

Major: Physics and Astronomy

Under the Supervision of Professor Ilya Kravchenko

Lincoln, Nebraska

May, 2019

SEARCH FOR RESONANT DOUBLE HIGGS PRODUCTION WITH BBZZ DECAYS IN THE $b\bar{b}\ell\ell\nu\bar{\nu}$ FINAL STATE IN pp COLLISIONS AT $\sqrt{s} = 13$ TeV

Rami Kamalieddin, Ph.D.

University of Nebraska, 2019

Advisers: Ilya Kravchenko

Since the discovery of the Higgs boson in 2012 by the A Toroidal LHC ApparatuS (ATLAS) and The Compact Muon Solenoid (CMS), most of the quantum mechanical properties that describe the long-awaited Higgs boson have been measured. Due to an impeccable work of the LHC, dozens of fb^{-1} of data have been delivered to both experiments. Finally, it became possible for analyses that have a very low cross section to observe rare decay modes of the Higgs boson, as was done successfully recently in ttH and VHbb channels. The only untouched territory is a double Higgs boson production. Data will not help us much either at the HL-LHC, the process will remain unseen even in the most optimistic scenarios, so one has to rely solely on new reconstruction methods as well as new analysis techniques. This thesis is addressing both goals. I have been blessed by an opportunity to work in the CMS electron identification group, where we have developed new electron identification algorithms. The majority of this thesis, however, will be devoted to the second goal of HL-LHC. We establish the techniques for the first ever analysis at the LHC that searches for the double Higgs production mediated by a heavy narrow-width resonance in the $b\bar{b}ZZ$ channel: $X \to HH \to b\bar{b}ZZ^* \to b\bar{b}\ell\ell\nu\bar{\nu}$. The analysis searches for a resonant production of a Higgs boson pair in the range of masses of the resonant parent particle from 250 to 1000 GeV. Both spin scenarios of the resonance are considered: spin 0 (later called "graviton") and spin 2 (later called "radion"). In the absence of the

evidence of the resonant double Higgs boson production from the previous searches, we set upper confidence limits. When combined with other search channels, this analysis will contribute to the discovery of the double Higgs production and we would be able to finally probe the Higgs boson potential using its self-coupling.

"... a place for a smart quote!"

Lenin, 1922.

ACKNOWLEDGMENTS

This will be a longgggg list!

Table of Contents

List of Figures

List of Tables

0.1 Introduction

In 2012, CMS [?] and ATLAS [?] collaborations officially discovered a Higgs-like particle and with that breakthrough the picture of the SM [?, ?, 38] of the particle physics has been completed. Most of the basic properties of the Higgs boson have been measured. However, it remains difficult to distinguish several processes with very low cross sections from the irreducible SM background processes with a similar signature. One such important but rare process is a double Higgs (HH) boson production. HH directly relates to the Higgs boson self-coupling, and thus, has an access to the shape of the Higgs boson potential. In the SM, HH production is a non-resonant process with a cross section of $\sigma =$ fb [?] at $\sqrt{s} = 13$ TeV.

Several Beyond the Standard Model (BSM) theories and models, such as supersymmetry, composite Higgs, Warped Extra Dimensions (WED) [?, 6–8, 10], predict scenarios when the double Higgs boson cross section is significantly increased and may be observed with the current data. There may be two different types of the BSM HH production: a non-resonant production, introducing BSM terms to the SM lagrangian or a resonant production, in which the process is mediated by a narrow width heavy mass resonance that subsequently would decay to SM Higgs bosons. [?].

In this analysis through the gluon fusion mechanism a heavy narrow resonance, such as RS1 KK graviton or RS1 radion ("graviton" or "radion" later in the text) [?,?,?] is produced. It decays to two Higgs bosons, which further decay to the bb pair (the first Higgs boson) and the ZZ/WW pair (the other Higgs boson). The analysis covers masses of graviton/radion from 250 GeV to 1000 GeV. Since no evidence of the signal has been reported by the previous HH analyses, we proceed directly to setting 95 % upper confidence limits on the production of the graviton with a subsequent decay to

Higgs bosons times the branching ratios of the Higgs boson decaying to a pair of b quarks and the other Higgs boson to two leptons and two neutrinos respectively (Fig. 0.1). We observe no deviation with the given data and evaluated uncertainties, the results are compatible with the Standard Model.

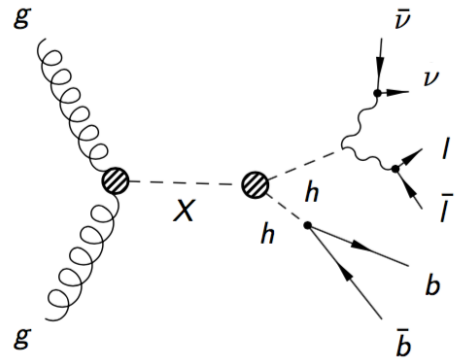

Figure 0.1: The Feynman diagram of the graviton/radion production with the subsequent decay to HH. HH system decays to a pair of b quarks and Z bosons. Shown is 2 b quarks, 2 leptons, and 2 neutrinos final state.

0.1.1 Analysis Strategy

The analysis is based on ntuples and object selection from the approved VHbb sister analysis [**?**]. Leptons, b jets, and the missing transverse energy (MET) are reconstructed using the standard CMS procedures [**?**] and the Particle Flow (PF) algorithm [**?**]. b-jets are identified using the Combined MVA v2 (CMVA) algorithm [**?**]. Then, on shell Z boson candidates are selected of dilepton pairs of the same flavour with a net charge zero for a pair. Higgs boson candidate decaying to b quarks (Hbb) is reconstructed as a pair of b jets with the highest CMVA output value. Finally, double Higgs boson pseudo-transverse mass, which is used in the shape analysis to extract limits, is constructed computing the transverse mass of the sum of the Lorentz vectors of the two leptons forming the on-shell Z, MET, and a pair of the b jets forming the

H $\rightarrow b\bar{b}$. Additionally, a cut on the missing transverse energy is introduced to preserves the orthogonality with the existing HIG-18-013 "2b 2l 2q" analysis, which also works with the $bbZZ$ decays. In a similar fashion, the cut on the Z mass ($m_Z > 76$ GeV) is used to orthogonalise the analysis with respect to the HH phase space used in the legacy $bbWW$ analysis where the final signature is identical to ours. Lastly, the cut on the BDT is used to reduce the background contamination in the signal region.

Main backgrounds are $t\bar{t}$ and Drell-Yan in association with jets. To determine their normalization, we construct two dedicated control region, which are correspondingly $t\bar{t}$ and Drell-Yan dominated. Then, during the the simultaneous fit of signal region (SR), as well as control region $t\bar{t}$ (CRTT), and control region Drell-Yan (CRDY), we obtain rates for these processes. Others, minor backgrounds, are single top production, diboson samples (WW, WZ, ZZ), and ZH production and are determined from the Monte Carlo (MC) simulation.

0.2 Data and Triggers

0.2.1 Data

This measurement uses the full dataset of 2016 collected with the CMS detector in pp collisions at 13 TeV center-of-mass energy with the corresponding integrated luminocity of 35.9 fb^{-1}.

As the measurement is based on dilepton signatures, the DoubleMuon and DoubleElectron primary datasets are analyzed and only on-shell $Z(\ell\ell)$ decays are considered, where $\ell =$,.

The run periods and the corresponding integrated luminosities are listed in Table 0.1 for DoubleMuon channel, DoubleElectron channel numbers are similar.

Table 0.1: List of used 2016 DoubleMuon data sets. An uncertainty of 2.5% is assigned for the 2016 data set luminosity [**?**]

Dataset	$\int L$ (fb^{-1})
DoubleMuon_Run2016B-03Feb2017-v2	∼5.9
DoubleMuon_Run2016C-03Feb2017-v1	∼2.7
DoubleMuon_Run2016D-03Feb2017-v1	∼4.3
DoubleMuon_Run2016E-03Feb2017-v1	∼4.1
DoubleMuon_Run2016F-03Feb2017-v1	∼3.2
DoubleMuon_Run2016G-03Feb2017-v1	∼3.8
DoubleMuon_Run2016H-03Feb2017-v1	∼11.8
Total Lumi	35.9

0.2.2 Triggers

Because the analysis is performed in the dielectron and dimuon channels, unprescaled dilepton triggers with the lowest available transverse momentum thresholds are utilized. The triggers at the level 1 (L1) and high level trigger (HLT) are listed in Table 0.2. Dielectron trigger requires the leading electron to pass 23 GeV p_T cut and the

trailing (subleading) electron to pass 12 GeV p_T cut, both electrons should be within $\eta < 2.5$. Dimuon triggers require the leading muon to pass 17 GeV p_T cut and 8 GeV p_T cut for the subleading muon, both muons should be within $\eta < 2.4$. The η region (1.4442 to 1.566) in the gap between the barrel and endcap is excluded.

Before measuring trigger scale factors, identification (ID) and isolation (ISO) cuts are applied, as well as p_T cuts of the offline selection. For dielectron trigger leading and subleading electrons have to pass 25 GeV p_T cut and 15 GeV p_T cut correspondinly. Dimuon triggers require the leading muon to pass 20 GeV p_T cut and 15 GeV p_T cut for the subleading muon. Dilepton scale factor have been computed for each leg separately, since the cuts on each leg vary (Fig. 0.2). Following the recommendations from the Muon POG, scale factors have been computed separately for two groups: run H and other runs, and then the final scale factors are determined as luminosity averaged scale factors (Figs. 0.3, 0.4, 0.5).

Muon ID, ISO, and electron ID+ISO scale factors are shown at Figs. **??**.

Table 0.2: Triggers for dimuon and dielectron analysis channels both at L1 and HLT levels.

Channel	L1 Seeds	HLT Paths
Z() Z()H $\to b\bar{b}$	L1_SingleMu20	HLT_Mu17_TrkIsoVVL_Mu8_TrkIsoVVL_v* OR HLT_Mu17_TrkIsoVVL_TkMu8_TrkIsoVVL_v* OR HLT_Mu17_TrkIsoVVL_Mu8_TrkIsoVVL_DZ_v* OR HLT_Mu17_TrkIsoVVL_TkMu8_TrkIsoVVL_DZ_v*
Z() Z()H $\to b\bar{b}$	L1_SingleEG30 OR L1_SingleIsoEG22er OR L1_SingleIsoEG24 OR L1_DoubleEG_15_10	HLT_Ele23_Ele12_CaloIdL_TrackIdL_IsoVL_DZ

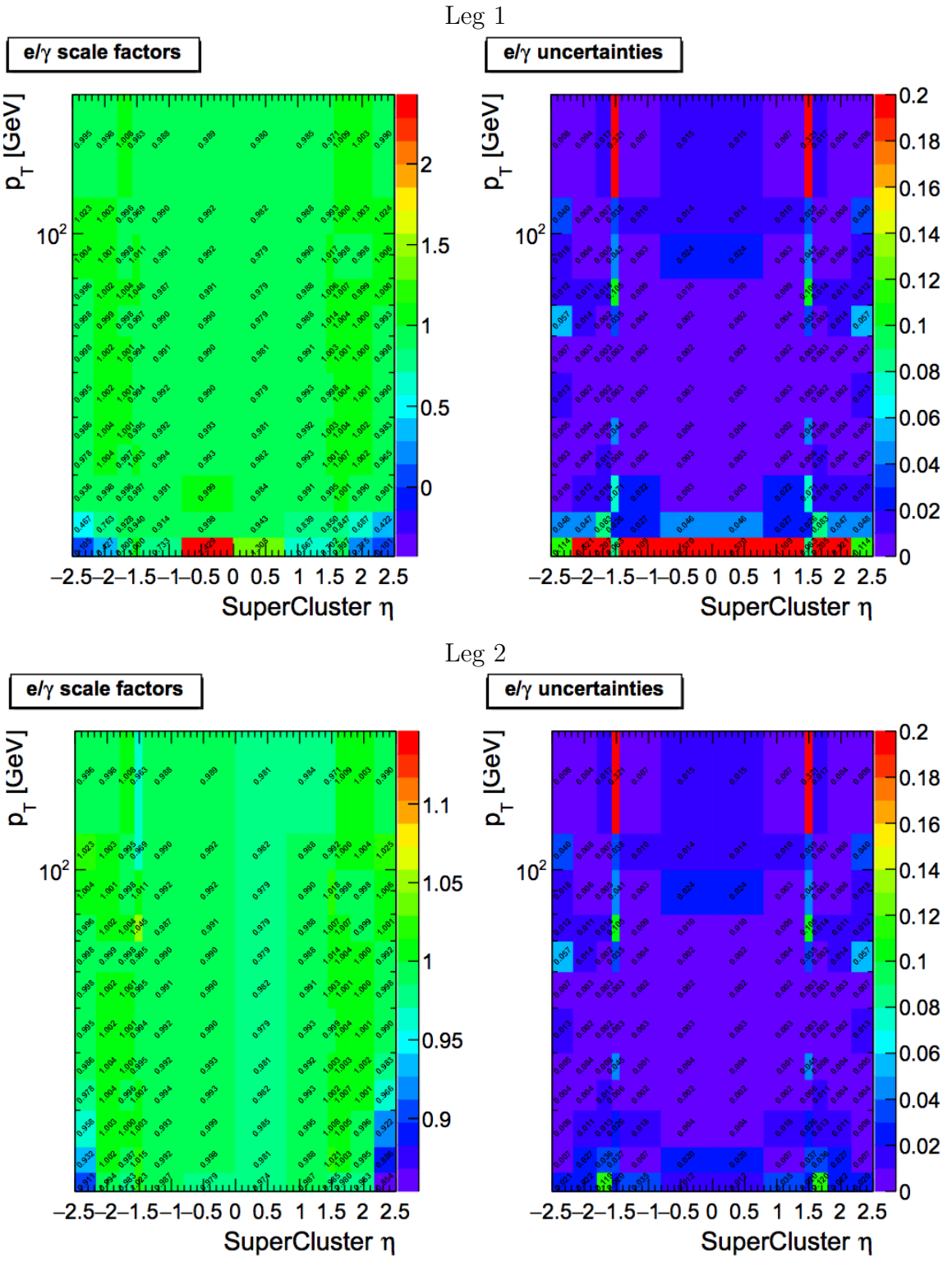

Figure 0.2: Electron scale factors in p_T and η bins for 2016 data set for the HLT_Ele23_Ele12_CaloIdL_TrackIdL_IsoVL_DZ trigger. ID cut (general purpose MVA WP90) and ISO cuts are applied, then the scale factors are measured. Taken from [**?**]

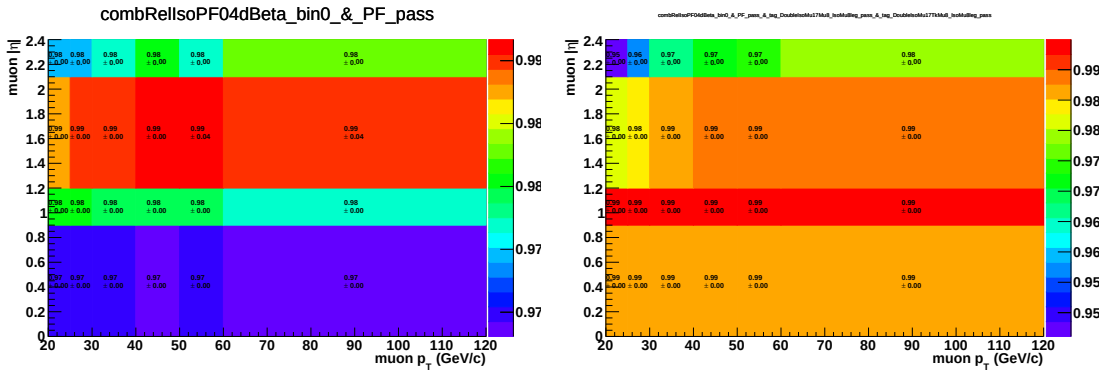

Figure 0.3: Muon scale factors in p_T and η bins for 2016 data runs B, C, D, E, F, G for the HLT_Mu17_TrkIsoVVL_Mu8_TrkIsoVVL_v* OR HLT_Mu17_TrkIsoVVL_TkMu8_TrkIs oVVL_v* triggers. Left: Scale factors for 8 GeV leg. Right: Scale factors for 17 GeV leg, provided that the subleading leg passed 8 GeV cut.

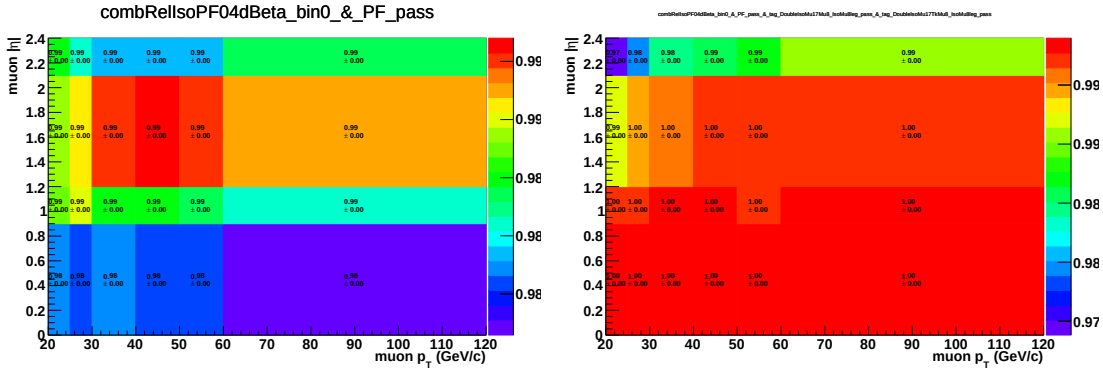

Figure 0.4: Muon scale factors in p_T and η bins for 2016 data run H for the HLT_Mu17_TrkIsoVVL_Mu8_TrkIsoVVL_v* OR HLT_Mu17_TrkIsoVVL_TkMu8_TrkIs oVVL_v* triggers. Left: Scale factors for 8 GeV leg. Right: Scale factors for 17 GeV leg, provided that the subleading leg passed 8 GeV cut.

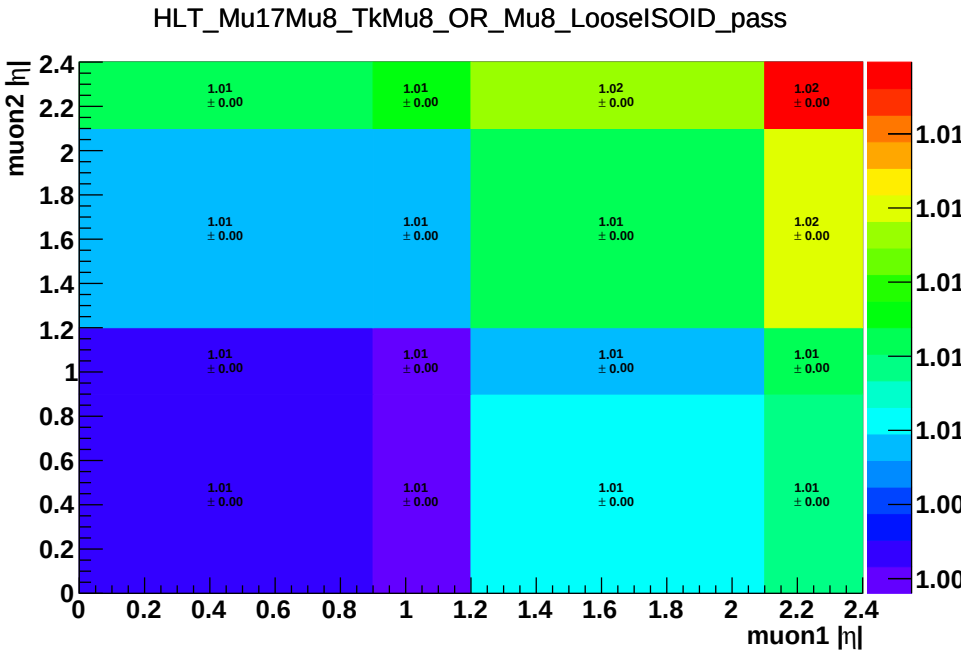

Figure 0.5: Scale factors in η bins of the leading and subleading muons for 2016 data set for dZ requirement, measured after muons have passed the HLT_Mu17_TrkIsoVVL_Mu8_TrkIsoVVL_v* OR HLT_Mu17_TrkIsoVVL_TkMu8_TrkIsoVVL_v* triggers.

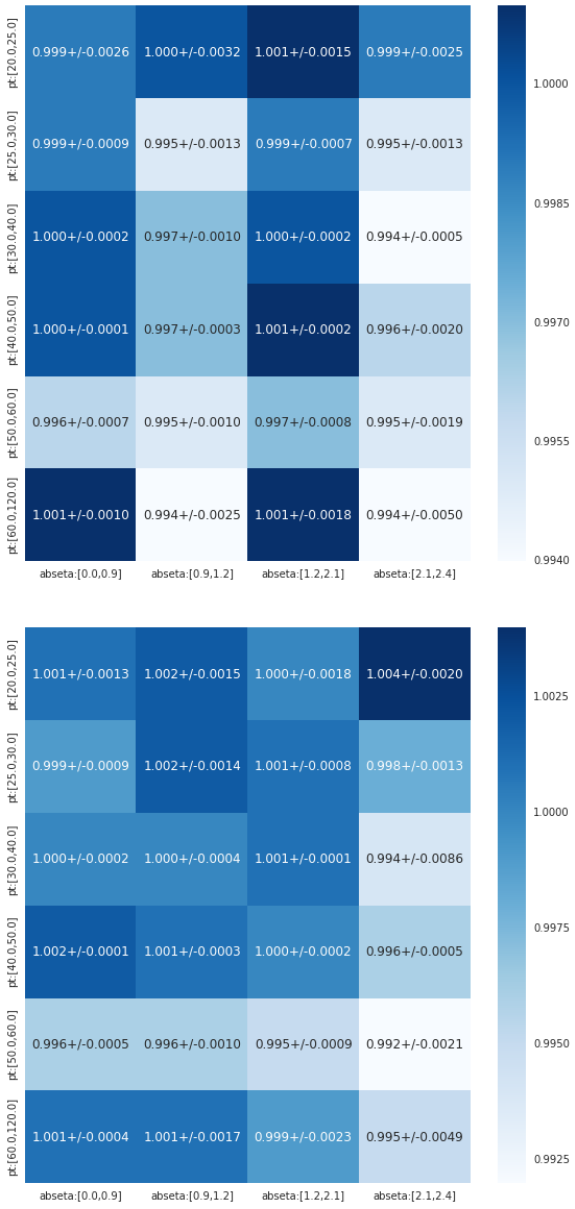

Figure 0.6: Muon ID scale factors in p_T and η bins. Left: runs B to F. Right: runs G and H.

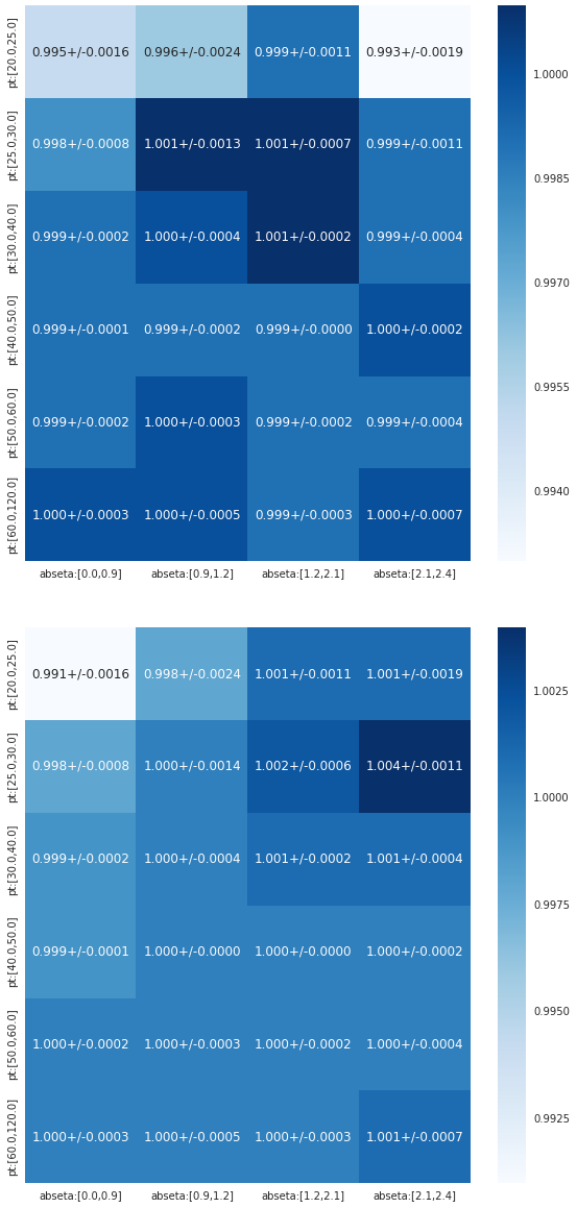

Figure 0.7: Muon ISO scale factors in p_T and η bins. Left: runs B to F. Right: runs G and H.

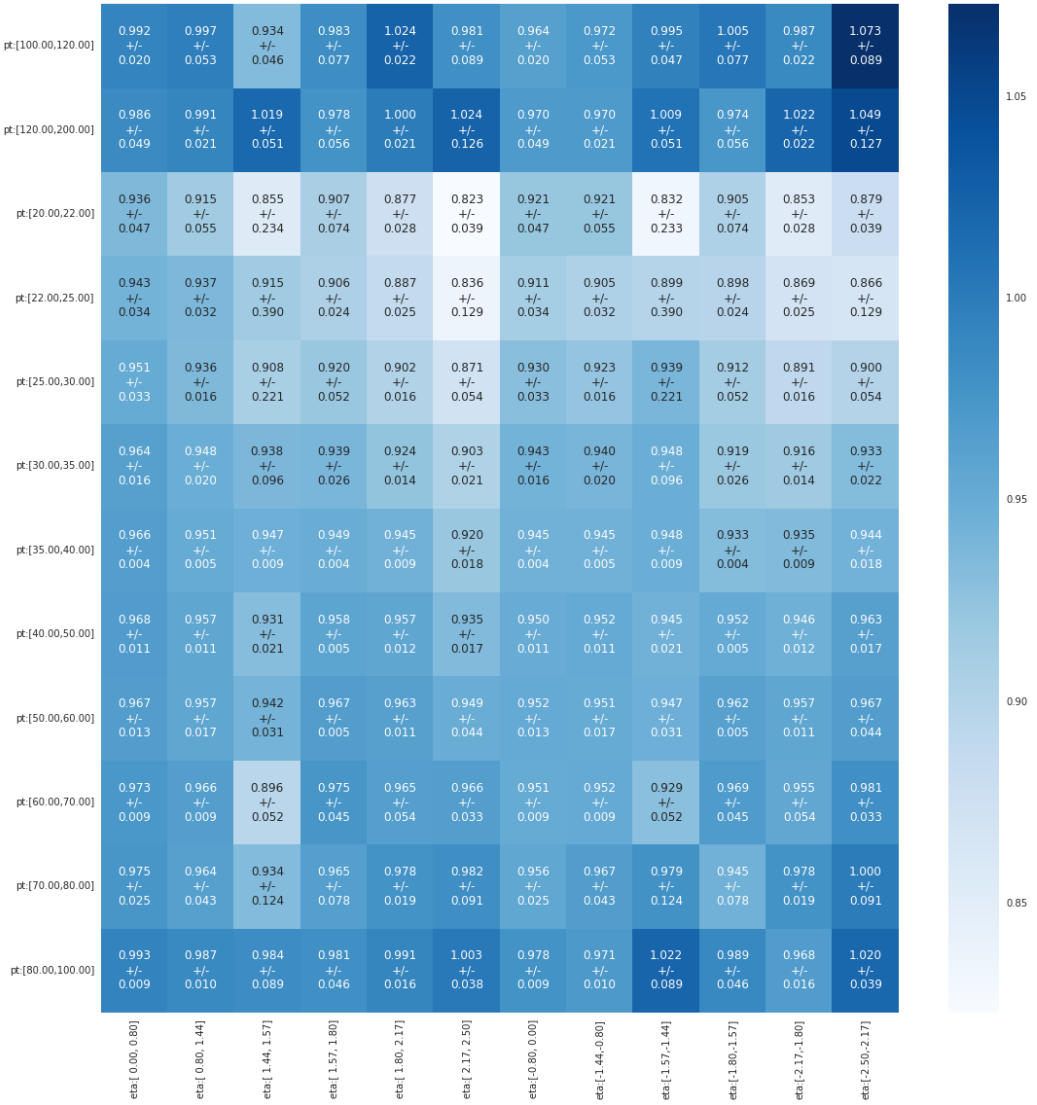

Figure 0.8: Electron ID+ISO scale factors in p_T and η bins.

0.3 Simulated Samples

0.3.1 Signal simulation

MC signal samples of the resonant Higgs boson pair production have been generated at the Leading Order (LO) using the 5 version 2.2.2.0 generator [**?**]. The gluon fusion production of a heavy narrow resonance is followed by the decay of the resonance into two SM Higgs bosons whose mass is fixed at 125 GeV.

Two signal MC samples are generated to cover the Higgs decay modes contributing to the 2 b jets 2 leptons 2 neutrinos final state of this measurement. The first sample type is a HH decay in to bbZZ channel, where one Higgs boson decays to a pair of b-quarks and the second Higgs boson decays into two Z bosons. In the second sample type bbVV events are generated, where HH can decay through bbWW and bbZZ channels. For both samples, the Z boson-pair and the W boson-pair are set to decay leptonically to two leptons and two neutrinos, where a lepton could be an electron or a muon. The second, bbVV, sample is filtered using the generator level information such that only the events with a W-boson pair (bbWW) are kept, while the Z-pair events are dropped: there are very few of them in the bbVV sample, and most importantly, high statistics bbZZ is taken from the dedicated bbZZ sample of the first type.

Events in the signal bbZZ and bbWW MC samples are normalised to 2 pb HH production cross section, which is a typical value of the heavy resonance production at 300 GeV predicted by the WED. Additionally the normalization includes the branching ratios of the Higgs boson decays contributing to the final state studied here: 0.0012 and 0.0266 for $HH \to bbZZ \to bb\ell\ell\nu\nu$ and $HH \to bbWW \to bb\ell\nu\ell\nu$, respectively [**?**].

Unless mentioned otherwise, throughout the text plots and numbers represent the

graviton study. The data and backgrounds for the radion measurement are the same, thus distributions also show the same good Data MC agreement and can be found for at Figs. 0.14 for the graviton case and 0.15 for the radion case.

0.3.2 Background simulation

In this analysis the main backgrounds are $t\bar{t}$ and Drell-Yan plus jets with the mass of the boson greater than 50 GeV. Not all the background processes pass our tight preselection (see section **??**), those which do, are single top, dibosons, and ZH backgrounds that are listed in the Table 0.3:

Table 0.3: Background Monte Carlo samples

DY1JetsToLL_M-50_TuneCUETP8M1_13TeV-madgraphMLM-pythia8
DY2JetsToLL_M-50_TuneCUETP8M1_13TeV-madgraphMLM-pythia8
DY3JetsToLL_M-50_TuneCUETP8M1_13TeV-madgraphMLM-pythia8
DY4JetsToLL_M-50_TuneCUETP8M1_13TeV-madgraphMLM-pythia8
WW_TuneCUETP8M1_13TeV-pythia8
WZ_TuneCUETP8M1_13TeV-pythia8
ZZ_TuneCUETP8M1_13TeV-pythia8
ZH_HToBB_ZToLL_M125_13TeV_aMC@NLO
TT_TuneCUETP8M1_13TeV-powheg-pythia8
ST_tW_top_5f_inclusiveDecays_13TeV-powheg-pythia8_TuneCUETP8M1
ST_tW_antitop_5f_inclusiveDecays_13TeV-powheg-pythia8_TuneCUETP8M1
ST_t-channel_top_4f_leptonDecays_13TeV-powheg-pythia8
ST_t-channel_antitop_4f_leptonDecays_13TeV-powheg-pythia8
ST_s-channel_4f_leptonDecays_13TeV-amcatnlo-pythia8

The simulated samples of the background processes such as $t\bar{t}$ [**?**] and the single top tW and t-channel production processes [**?**] are generated at the next-to-leading order (NLO) with POWHEG [**?**], while single top s-channel production process is generated at NLO with . $t\bar{t}$ and single top production cross sections are rescaled to the next-to-next-to-leading order (NNLO). Drell-Yan (DY) process samples in

association with 1, 2, 3 or 4 jets are generated at the leading order using with the MLM matching [**?**] and rescaled to NNLO using FEWZ program [**?**, **?**, **?**].

As for the electroweak (EWK) order, DY samples have been rescaled to EWK NLO order with the NLO/LO k-factor of 1.23 [**?**]. Diboson samples are generated at LO with 8.212 [**?**].

The main background process, which involves SM Higgs boson, is an associated production of the Higgs boson with a Z boson (ZH). ZH process is simultated using the generator $MadGraph5\_aMC@NLO$ [**?**] with FxFx merging [**?**] and rescaled to NNLO with generator [**?**].

For LO and NLO samples NNPDF3.0 parton distribution functions (PDF) set is used. and interfaced with 8.212 [**?**] are used for the parton showering and hadronization steps. To describe the underlying event CUETP9M1 set derived in [**?**] is used. [**?**] is used to model the response of the CMS detector.

All the final cross sections denoted as NNLO are calculated at NNLO QCD accuracies and have been computed with the tool they were generated with. They found to be in agreement with the values from the LHC Higgs cross section working group [**?**, **?**, **?**, **?**, **?**].

During the data taking in 2016 the average number of proton-proton interactions per bunch crossing was 24 (denoted as pile up later), and in MC samples this information has been introduced overlapping these interactions with the events of interest.

0.4 Physics Objects Reconstruction

This the first ever bbZZ analysis performed at CERN with the real data uses the standard set of the CMS reconstructed physics objects. We describe reconstruction of electrons, muons, jets and b jets, and MET separately below:

0.4.1 Electrons

The Gaussian Sum Filter algorithm (GSF Electrons) [**?**] is used to reconstruct electrons. GSF helps to estimate track parameters. The procedure starts as follows: a mixture of Gaussian distributions (normally about 4-6 components) [**?**] is used to estimate the energy loss in each layer of the tracker. The energy loss is modelled by the Bethe-Heitler formula. Two most important track properties are then computed: a weighted mean or the most frequent value (mode). The first estimate is unbiased while the latter one has a smaller width. In practice, mostly one works with the mode. Gaussian mixtures are determined minimising either the absolute difference between the CDFs of the model and of the Gaussian mixture, or the Kullback-Leibner distance, which is a logarithm of the ratio of the pdfs of the model with respect to the mixture. Finally, the tracks are extrapolated further to the ECAL The measurement selects electrons, which pass the following selection: leading electron $p_{\mathrm{T}} > 25$ and subleading electron $p_{\mathrm{T}} > 15$, $|\eta| < 2.5$, an isolation cut of 0.06, for which the cone of 0.3 is used to compute the ρ-subtracted PF isolation. Lepton isolation is calculated as a scalar sum of the transverse momentum (p_T) of all the charged and neutral hadrons as well as photons around the lepton (excluding the cone) normalised to the p_T of the lepton itself.

On top of the selection defined above, a specific CMS Particle Object Group (POG) recommended working point (WP) is applied, which is a discriminant based

on the a multivariate analysis (MVA) for classification of signal/background electrons. The WP consists of nearly 20 variables utilising the information from the impact point, tracks, and the ECAL: $\chi^2 variables$ of the track and the quality of its estimate, $\delta\eta$, $\delta\phi$, energy of the 3 by 3 cluster, ECAL energy over momentum, etc. For this analysis we use the loose working point (another name can be WP90), as described in [**?**]. ID and ISO, as well as the HLT SFs are applied.

0.4.2 Muons

In this analysis we are using global muons reconstructed using the information from the tracker and muon system [**?**,**?**]. During the offline reconstruction, muons chambers segments are used as seeds for the "standalone muon" reconstruction. The seed is a position, a direction, and an initial momentum of the muon candidate. This serves as an input to the track fitting procedure utilising muon system information. The resulting object after executing this technique is what is called a standalone muon. Then, for each standalone muon the algorithm searches for the tracks reconstructed in the inner tracking system (tracker tracks) that would match the muon. Then for each standalone muon - tracker track pair the Kalman filter based fit [**?**] is performed. The result is a collection of muons which are referred to as global muons. In this analysis the kinematic and isolation selection of global muons is the following:

leading muon $p_{\mathrm{T}} > 20$ and subleading muon $p_{\mathrm{T}} > 15$, $|\eta| < 2.4$, a relative isolation cut of 0.15, with the cone of 0.4 used to compute $\Delta\beta$-subtracted PF isolation. Finally, a tighter selection - muon POG recommended WP Loose is applied [**?**, **?**]. WP consists of track quality information: χ^2 of various fits, number of good hits in the tracker, number of layer missing the expected hit, impact parameter variables, matching variables (e.g., a segment in the muon station matched to the tracker track

extrapolation), compatibility variables (e.g., a muon segment compatibility). ID, ISO, HLT and tracker SFs are applied.

0.4.3 Jets

Particle flow (PF) algorithm is used to reconstruct jets [**?**, **?**], with the help of the anti$-k_T$ clustering algorithm having a distance parameter of $R = 0.4$ [**?**, **?**]. Jets are collimated bunches of stable hadrons originating from quarks and gluons after fragmentation and hadronization. Therefore, jet finding procedure is a back-propagation that starts with the detected objects and following the rules of the quantum mechanics for fragmentation and hadronization targets to identify the initial partons. anti-k$_T$ is a sequential clustering algorithm that first defines the notion of the distance between the two particles in the collection of particles of the event, and also a distance between the particle and the beam axis. Then sequentially iterating over the particles collection it computes the smallest distances, if the smallest one is between the particles, their 4-momentum is combined into one. If the smallest distance is between the particle and the beam axis, then the particle is called the jet, removed from the collection, and the whole procedure continues. anti-k$_T$ is known to be insensitive to the underlying event and to the pile up, therefore, is commonly used.

Reconstructed jets are further corrected for detector effects using specific corrections determined from the data and MC. Only jets passing $|\eta| < 2.4$ and ($p_{\mathrm{T}} > 30$) are considered for the analysis. All the necessary jet energy resolution (JER) and jet energy scale (JES) corrections provided by the JetMET group are applied [**?**].

0.4.4 Identification of b jets

MVA technique combining the information about the impact parameter, identified secondary vertices, as well as soft lepton (if any) contained inside of the jet is used by the CMVA algorithm to identify b quark originated jets. The output is a continuous MVA discriminant ranging in value from -1 to +1. Optimal cut is determined by the POG for several working points. We use CMVAv2 medium working point (> 0.4432). We checked all three WPs and WP Medium gives the best limits. b tagging and mistagging corrections are applied.

0.4.5 Missing transverse energy

Even though neutrinos leave no trace in the CMS detector, their presence may be inferred through the momentum imbalance. A quantity reconstructed in this fashion in the plane perpendicular to the beam axis is called a missing transverse energy/momentum (MET). Precise reconstruction of leptons, photons, jets, etc is necessary for the correct computation of the MET. Detector miscalibration and PU also affect MET performance, thus the studies with the real data are always conducted.

Due to the conservation of the momentum in the transverse plane, MET can be calculated as an absolute value of the negative vectorial sum of the transverse momentum of all observed particles: $\overrightarrow{E_T} \equiv -\sum \overrightarrow{p_T}$

MET reconstructed using PF is what the majority of the CMS teams uses for analyses of 2016 data. Several correction recommended by the JetMET POG are applied [**?**]: jet corrections, corrections for the PU effect, etc. On top, a set of filters related to the instrumental effects is employed, such as removal of the misreconstruction caused by the fisfier in the HCAL and/or noice in the tracker, etc. [**?**]. Schematic representation of the MET in the event with Z or photon is shown on the Fig. 0.9.

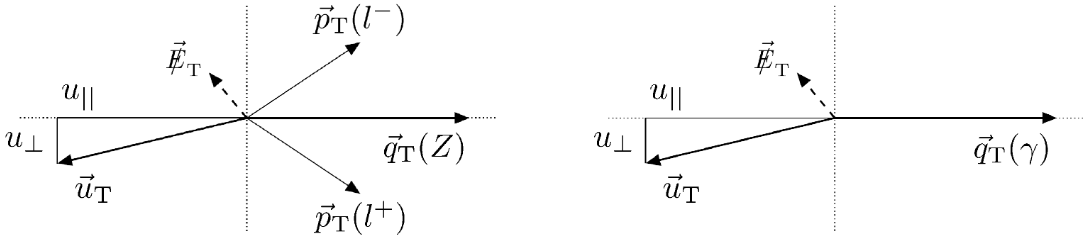

Figure 0.9: Z boson (left) and photon (right) kinematics with the vector of all the visible objects (denoted by u) and a resulting MET.

0.5 Event Selection

0.5.1 Higgs and Z Boson Selection

Only dilepton pairs having net charge of zero are considered as $Z \to \ell\ell$ candidates. Pairs of prompt isolated leptons must have a dilepton mass greater than 76 GeV. This ensures the orthogonality with HIG-17-006 bbVV analysis (later also referred to as bbWW analysis) as well as helps selecting decays of real Z bosons.

Higgs boson candidates are reconstructed from the b jet pairs utilising the two b jets with the highest CMVAv2 discriminant value. We do not veto additional b jets as with the increased PU growths the probability to have more b jets.

Double Higgs boson candidate is computed as a sum of Lorentz vectors of the $Z \to \ell\ell$ candidate, MET, and a $H \to b\bar{b}$ candidate. Then, we compute the transverse mass of that object.

Transverse mass definition that we follow is one of the commonly used and is logical in the sense that we subtract the longitudinal momentum component which leaves us with the transverse momentum components only (while the energy remains the total energy).

More precisely, as the z-component of the neutrinos' momentum is unknown and for various reasons we do not attempt to reconstruct it, we form a pseudo transverse mass:
$\tilde{M}_T(HH) = \sqrt{E^2 - p_z^2}$ (further referred as transverse mass for brevity), where E and p_z are the energy and the z-axis component of the Lorentz energy-momentum vector of the HH candidate.

The resulting distribution, $\tilde{M}_T(HH)$, is what will be used in the binned shape analysis with the Higgs Combination Tool following the section "Binned shape analysis" as described at the twiki [**?**]. Shape analysis is more sensitive than the simple cut-

and-count experiment (one bin distributions) since more information/discrimination power is given to the likelihood function.

Initial data files, called ntuples, have enormous size of the order of more than a Terabyte per background process. To reduce the size of the ntuples and remove obvious background events (to remove signal-like events we apply a sophisticated selection and use a BDT), we apply a "common-sense" HH preselection. It starts with the requirement on dilepton mass be greater than 50 GeV and the event to contain at least two "good" jets - with $p_T > 30$ GeV and $|\eta| < 2.4$. In addition to requirements on Higgs bosons decaying to b quarks mentioned above, we define Z bosons as two opposite sign muons with $p_T > 20/15$ GeV (leading/subleading lepton) or two opposite sign electrons with $p_T > 25/15$ GeV (leading/subleading lepton).

Later analysis cuts, the selection chain to improve signal-background separation, include:

- the requirement of at least two b jets in the event, out of which two with the highest CMVAv2 score are used to define H $\rightarrow b\bar{b}$ candidate
- the lower end cut on the H $\rightarrow b\bar{b}$mass set to 20 GeV to remove the low mass resonances, while giving BDT as many events in the CRDY as possible at the same time. The upper end cut is not explicitly set for the same purpose. The actual H $\rightarrow b\bar{b}$mass distribution after the analysis selection is concentrated in the range 30 to 220 GeV
- the Z boson selection takes the most energetic two leptons of the opposite sign and requires their dilepton mass to pass 76 GeV < Z mass < 106 GeV condition used for the signal region definition. This is a standard $\pm$ 15 GeV window for Z boson selection whose lower end also preserves othogonality with the existing HIG-17-006 bbVV analysis

- HH candidate is approximated by the sum of , Z, and H $\rightarrow b\bar{b}$ decays. A loose cut on HH transverse $>$ 100 GeV removes evidently background events

- finally, an additional set of cuts is used to ensure orthogonality with the existing HIG-18-013 bbZZ analysis focusing on the 2b jets + 2 leptons + 2 quarks, see Table 0.4. The MET cuts have been optimised by both analysis to yield the best limit when the results of two measurements are combined.

Table 0.4: cut to orthogonalise the analysis with respect to HIG-18-013.

Signal mass, GeV	cut, GeV
260-300	> 40
350-600	> 75
650-1000	> 100

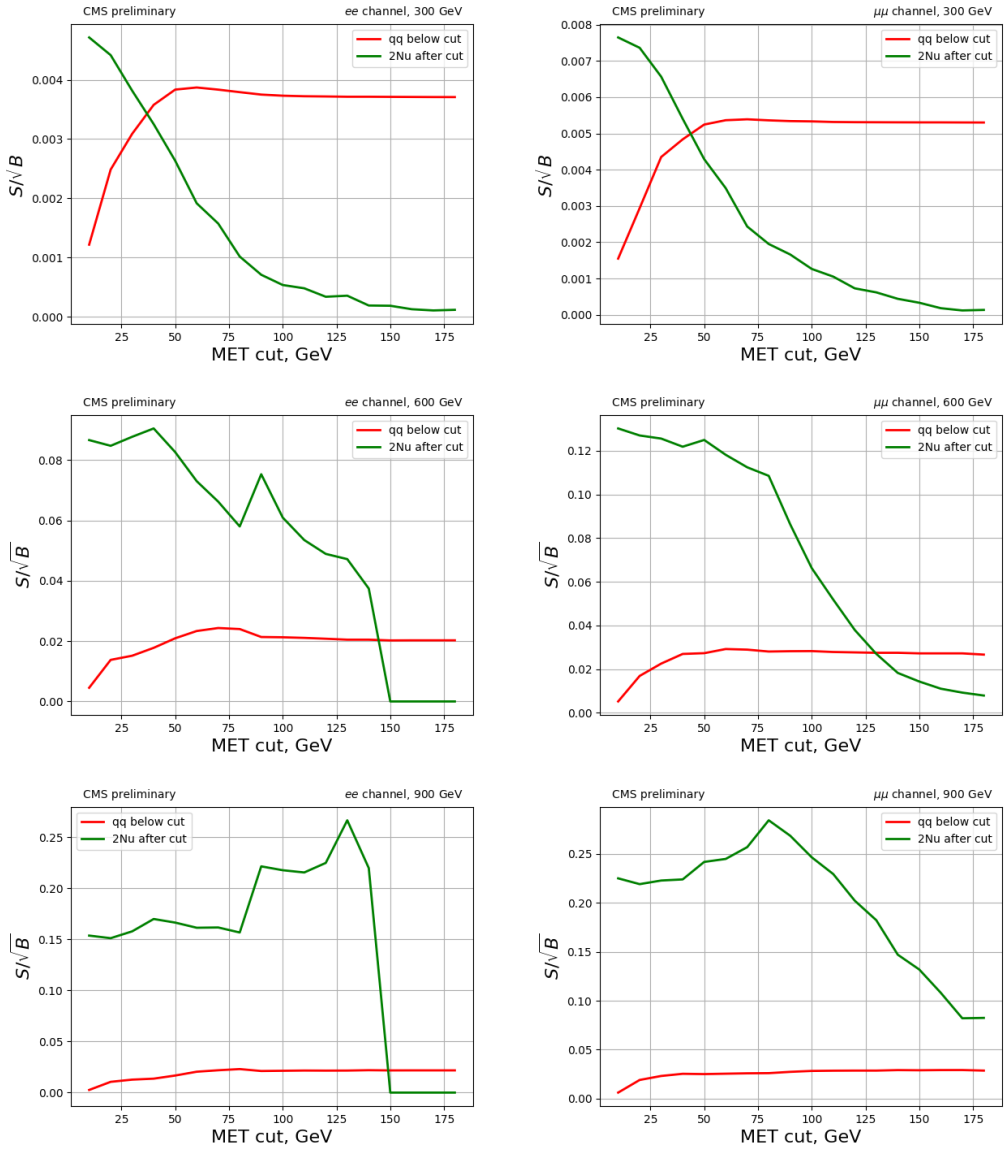

Figure 0.10: Significance-like ($\sqrt{S}/B$) figure of merit as a function of the MET cut. Green curve shows the significance for our analysis keepings event above the cut, red curve is for HIG-18-013 analysis and their phase space is below the cut value. Top: 300 GeV cut. Middle: 600 GeV cut. Bottom: 900 GeV cut. On the left dielectron channel is shown, while dimuon plots are on the right.

0.5.2 H $\to b\bar{b}$ and Z $\to \ell\ell$ variables to define signal and control regions

In this analysis we define three regions in the H $\to b\bar{b}$ and Z $\to \ell\ell$ space. Two regions, CRDY and CRTT, are used to extract the normalization of corresponding backgrounds. Signal region (Fig. 0.11) is chosen by the set of H $\to b\bar{b}$ and Z $\to \ell\ell$ cuts 0.11. To reduce background contamination in this region, an additional cut on the MVA output is used. Boosted decision trees (BDT) MVA technique is employed to separate background from signal. Below we describe in details selection of each region and BDT construction.

For CRDY we invert H $\to b\bar{b}$ cut, keeping in the lower sideband only events with the mass of Higgs boson higher than 20 GeV to avoid fakes from QCD. For CRTT we invert Z $\to \ell\ell$ cut, keeping only high mass sideband to ensure the orthogonality with the existing HIG-17-006 bbVV analysis.

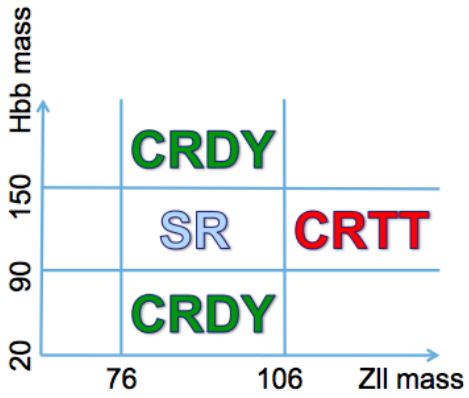

Figure 0.11: Signal region, control region $t\bar{t}$, and control region Drell-Yan in the phase space of Z $\to \ell\ell$ and H $\to b\bar{b}$ masses.

Table 0.5: Efficiency of the BDT selection requirement. ee channel (top) and mm channel (bottom).

sample	Efficiency at 300 GeV, [%]	Efficiency at 900 GeV, [%]
signal (bbZZ)	89.2	94.9
signal (bbWW)	75.0	88.4
$t\bar{t}$	28.8	0.2
Drell-Yan	74.2	1.2
Single top	33.1	1.1
ZH	88.8	10.7
Dibosons	90.0	5.0
sample	Efficiency at 300 GeV, [%]	Efficiency at 900 GeV, [%]
signal (bbZZ)	58.1	91.1
signal (bbWW)	25.9	96.3
$t\bar{t}$	13.6	0.2
Drell-Yan	39.0	0.8
Single top	13.0	0.2
ZH	56.0	8.4
Dibosons	51.4	6.2

	signal_hzz	signal_hww	ZH	TT	ST	VV	DY	exp limit
300_new	0.17	0.02	26.72	442.44	10.05	26.44	833.74	796.88
300_old	0.15	0.03	13.50	403.24	8.62	26.38	609.15	696.88
451_new	0.17	0.03	5.81	7.73	1.29	4.87	35.25	97.19
451_old	0.16	0.04	3.14	6.60	1.31	4.93	24.42	92.58
900_new	0.54	0.13	2.20	2.70	0.29	1.50	9.91	13.71
900_old	0.52	0.14	1.64	2.70	0.29	1.50	8.29	12.23

Figure 0.12: Yields for ee channel before and after the tight isolation bug fix in the HEPPY. The effect is minimal as can be seen in the final limit.

0.5.3 Signal and background characteristics

The signal region is further purified applying the cut in the BDT output (Table 0.5 contains the efficiency numbers for the BDT cut). The first set of BDT variables in the early version of the analysis included 30-50 variables, which could potentially discriminate signal from the background. The set contained variables related to the kinematical properties of the signature, as well as a dozen of angular variables. After the first optimization, nine best variables were determined and chosen to be used for the analysis. Removal or addition of other variables did not improve the performance.

Following the procedure adopted by matured HH analyses, we split the mass range into two: low mass and high mass (á la HIG-17-002 and HIG-17-008). These simplification costs some performance loss but allows analysis to proceed with just two BDTs instead of training one BDT per mass point, which would require more than a dozen of trainings per heavy resonance, though, training a dedicated BDT for each signal mass hypothesis would give a better performance. However, the adopted path saves computational resources. Another reason is impracticality, bbZZ signature is not the most sensitive, bb$\gamma\gamma$ is and the difference in sensitivity is a factor of 30-100 depending on the mass. More in the chapter 0.6. The low/high mass boundary value for HH analyses is chosen typically in the range 300-450 GeV. In our case the performance of the boundary around 300 GeV (area under the ROC curve for low mass BDT is 0.9138 and 0.9805 for high mass BDT) is similar to the boundary option at the 450 GeV (area under the ROC curve for low mass BDT is 0.9086 and 0.9957 for high mass BDT), and to the one in the middle of the range (area under the ROC curve for 400 GeV for low mass BDT is 0.9074 and 0.9928 for high mass BDT). Therefore, we chose the value of 450 GeV, which is also a choice of the bbbb analysis [**?**]. Upon running the full chain up to analysis limits, the choice of 450 GeV was confirmed to

Table 0.6: Number of events surviving analysis cuts corresponding to the last entry in the 0.13 .

Process, mass point	ee channel, %	mm channel, %
bbZZ, 300 GeV	2256	4511
bbWW, 300 GeV	53	85
bbZZ, 900 GeV	8034	12963
bbWW, 900 GeV	12	23

be the best split point option. As a result, the low mass BDT includes a mix (with the weight '1') of seven signal samples: 250, 260, 270, 300, 350 400, 450 GeV. The high mass training includes nine masses: 500, 550, 600, 650, 700, 750, 800, 900, 1000. In each case the composition of the background is the same, it is a mix (by cross section) of $t\bar{t}$ and Drell-Yan plus jets.

Cut flow for ee and mm channels from the gen level up to before the BDT selection is shown on the figures 0.13. In the cut flow table 0.13 the following definitions are used: very loose selection means all GsfElectrons and Muons from the basic collections that match gen-level electrons/muons and pass the very minimal kinematic cuts; loose selection means loose POG selection consisting of kinematic, dxy/dz, iso cuts. The final efficiency values represent these numbers in terms of events 0.6:

0.5.3.1 Data and MC comparison

Signal region BDT side-band plots as well as unblind signal region plots show good data-MC agreements. We are not cutting on BDT for control regions, therefore, all the mass point have the same background and data distributions. That is why we provide below plots for two mass points: one mass point representing low mass region, 300 GeV, and one mass point representing high mass region, 900 geV. Signal bbZZ and bbWW rates for all plots are multiplied by some high factors depending on the mass point purely for the visualization purpose and do not go in the real analysis.

	2 very loose muons	2 loose muons	mva ID	leading pt and eta gap	iso<0.15	trigger	>=2b-jets, Hbb and Zll cuts
bbWW300	100.0	41.8	21.6	20.3	17.8	16.6	0.2
bbZZ300	100.0	87.4	61.6	56.7	43.0	40.7	10.4
bbWW900	100.0	53.5	15.8	14.6	10.5	9.9	0.1
bbZZ900	100.0	84.0	63.3	59.7	53.6	50.2	15.1

	2 very loose electrons	2 loose electrons	mva ID	leading pt and eta gap	iso<0.06	trigger	>=2b-jets, Hbb and Zll cuts
bbWW300	100.0	38.8	18.9	17.4	13.0	10.0	0.1
bbZZ300	100.0	68.2	46.3	43.9	24.7	23.1	5.9
bbWW900	100.0	38.5	14.9	13.1	5.5	4.8	0.0
bbZZ900	100.0	71.4	46.0	43.7	36.0	33.9	10.0

Figure 0.13: Cut flow for mm (top) and ee (bottom) channels.

Prefit plots are available in the Appendix **??**. Control regions only postfit plots have been produced during an extensive discussion with Higgs conveners at Hyper-News, and it was shows that upon inclusion of the SR in the fit the data-MC agreement is slightly better. Postfit plots that include SR in simultaneous fit, hence a common jargon name "Full postfit" plots, are presented at the figures **??** - **??** and show data and MC comparison in the SR, CRDY, and CRTT. For both ee and mm channels, low and high mass regions. The latest style plots produced for the PAS can be found at Fig. 0.14 for the graviton case and Fig. 0.15 for the radion case.

Distributions of nine variables that go into the BDT have been studied in depth during the pre-approval process and are available in the Appendix **??**. After the tight isolation cut fix in the HEPPY framework the results/shapes are almost unchanged (it is also can be observed from the table of yields 0.12). At the yields table 0.12, 450 GeV mass point, since evaluated using the high mass BDT, is called 451 GeV for clarity purposes.

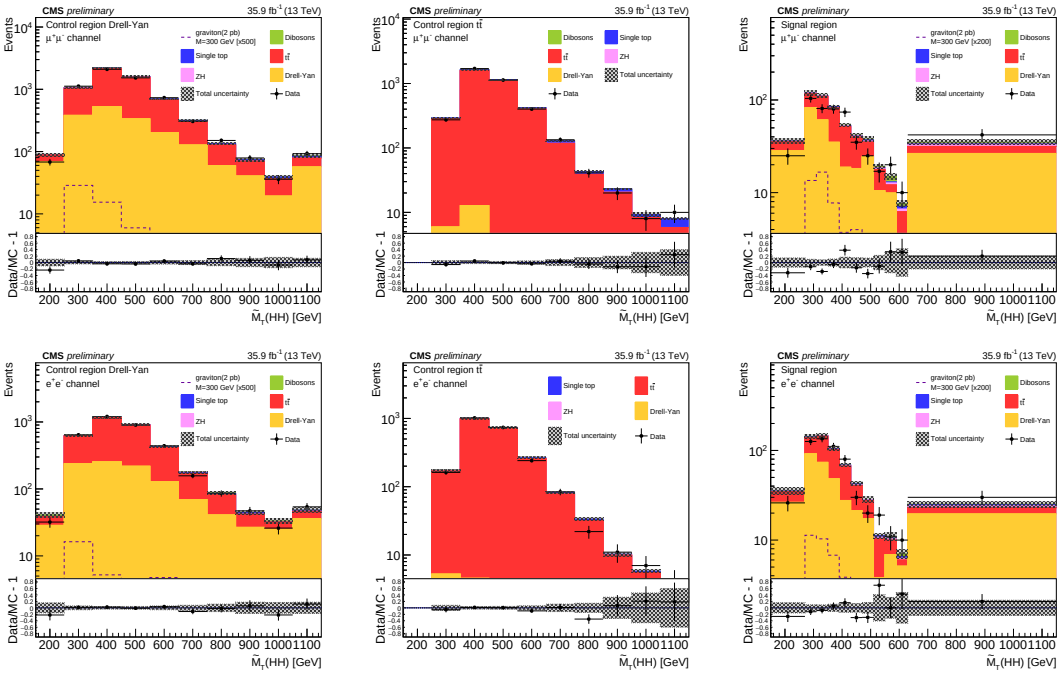

Figure 0.14: Transverse mass of the reconstructed HH candidates for data, the simulated signal graviton sample for the 300 GeV mass hypothesis, and simulated backgrounds scaled according to the fit results. The top row shows the figures for the muon channel while the bottom row is for the electron channel. For each row, the left plot is for the Drell-Yan control region, the middle is for the $t\bar{t}$ control region, and the right is for the signal region. Signal normalization choice is discussed in the text. The crosshatched area represe nts the sum of statistical and systematic uncertainties.

0.5.3.2 Scale Factors

Electron ID and ISO scale factors, as well as HLT scale factors (Fig. 0.2), have been computed by VHbb group and presented at the EGamma physics object groups (POG) meeting [**?**]. Muon ID scale factors, as well as ISO scale factors, have been derived separately for runs G/H and B/C/D/E/F runs and then luminosity averaged [**?**]. Tracker scale factors (0.2) are taken from the Muon POG twiki [**?**]. HLT dimuon scale factors were derived by VHbb group and further approved by the muon POG. These scale factors were derived separately for run H (Fig. 0.4) and B/C/D/E/F/G (Fig. 0.3) runs and then luminosity averaged [**?**]. On top, separate scale factors

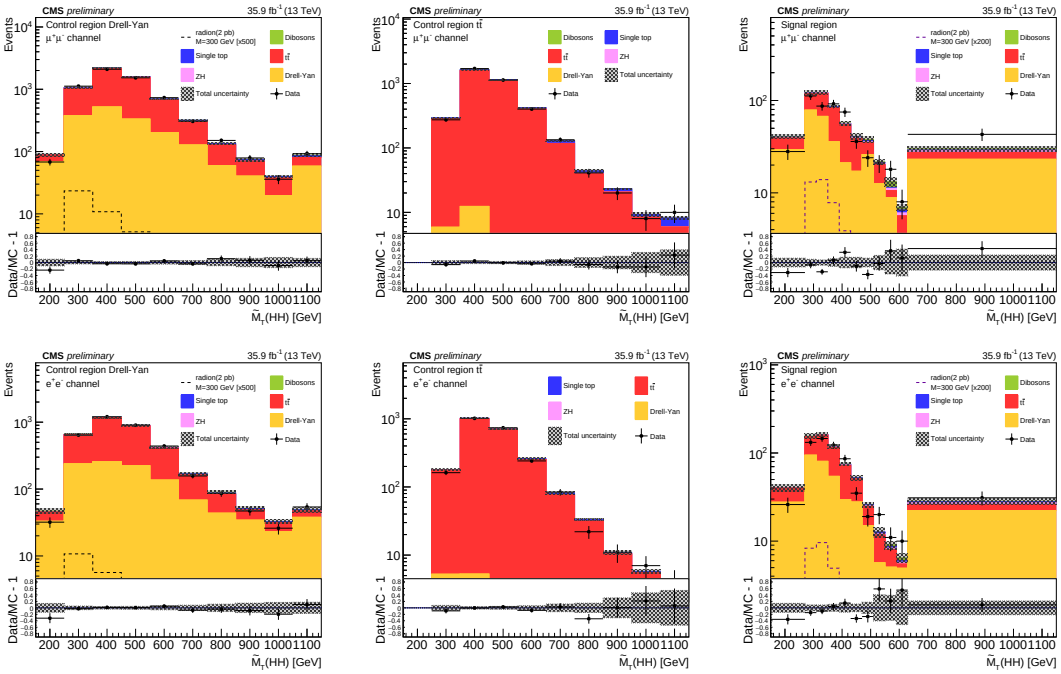

Figure 0.15: Transverse mass of the reconstructed HH candidates for data, the simulated signal radion sample for the 300 GeV mass hypothesis, and simulated backgrounds scaled according to the fit results. The top row shows the figures for the muon channel while the bottom row is for the electron channel. For each row, the left plot is for the Drell-Yan control region, the middle is for the $t\bar{t}$ control region, and the right is for the signal region. Signal normalization choice is discussed in the text. The crosshatched area represe nts the sum of statistical and systematic uncertainties.

are calculated for the dZ requirement of HLT_Mu17_TrkIsoVVL_Mu8_TrkIsoVV L_DZ_v* OR HLT_Mu17_TrkIsoVVL_TkMu8_TrkIsoVVL_DZ_v* triggers, us- ing dilepton events that have already passed the HLT_Mu17_TrkIsoVVL_Mu8_TrkIsoVVL_v* OR HLT_Mu17_TrkIsoVVL_TkMu8_TrkIsoVVL_v* triggers (Fig. 0.5).

0.6 BDT Discriminant

0.7 Systematic Uncertainties

0.8 Statistical Analysis

0.9 Limits Extraction

0.10 Conclusions

References

[1] Matthias U. Mozer. Electroweak Physics at the LHC. *Springer Tracts Mod. Phys.*, 267:1–115, 2016.

[2] Gennadi Sardanashvily. *Noether's theorems: applications in mechanics and field theory*. Atlantis studies in variational geometry. Springer, Paris, 2016.

[3] Steven Weinberg. The Making of the Standard Model. *Eur. Phys. J. C*, 34(hep-ph/0401010):5–13. 21 p. ; streaming video, 2003.

[4] Roger Wolf. *The Higgs Boson Discovery at the Large Hadron Collider*, volume 264. Springer, 2015.

[5] Jose Andres Monroy Montanez, Kenneth Bloom, and Aaron Dominguez. Search for production of a Higgs boson and a single Top quark in multilepton final states in pp collisions at $\sqrt{s} = 13$ TeV, Jul 2018. Presented 23 Jul 2018.

[6] Peisi Huang, Aniket Joglekar, Min Li, and Carlos E. M. Wagner. Corrections to di-Higgs boson production with light stops and modified Higgs couplings. *Phys. Rev.*, D97(7):075001, 2018.

[7] Matthew J. Dolan, Christoph Englert, and Michael Spannowsky. New Physics in LHC Higgs boson pair production. *Phys. Rev.*, D87(5):055002, 2013.

[8] Shinya Kanemura, Kunio Kaneta, Naoki Machida, Shinya Odori, and Tetsuo Shindou. Single and double production of the Higgs boson at hadron and lepton colliders in minimal composite Higgs models. *Phys. Rev.*, D94(1):015028, 2016.

[9] Albert M Sirunyan et al. Search for Higgs boson pair production in the $\gamma\gamma b\bar{b}$ final state in pp collisions at $\sqrt{s} = 13$ TeV. 2018.

[10] Alexandra Oliveira. Gravity particles from Warped Extra Dimensions, predictions for LHC. 2014.

[11] Lisa Randall and Raman Sundrum. A Large mass hierarchy from a small extra dimension. *Phys. Rev. Lett.*, 83:3370–3373, 1999.

[12] Kunihito Uzawa, Yoshiyuki Morisawa, and Shinji Mukohyama. Excitation of Kaluza-Klein gravitational mode. *Phys. Rev.*, D62:064011, 2000.

[13] H. Davoudiasl, J. L. Hewett, and T. G. Rizzo. Phenomenology of the Randall-Sundrum Gauge Hierarchy Model. *Phys. Rev. Lett.*, 84:2080, 2000.

[14] Michael Forger and Hartmann Romer. Currents and the energy momentum tensor in classical field theory: A Fresh look at an old problem. *Annals Phys.*, 309:306–389, 2004.

[15] Chuan-Ren Chen and Ian Low. Double take on new physics in double Higgs boson production. *Phys. Rev.*, D90(1):013018, 2014.

[16] Roberto Contino, Margherita Ghezzi, Mauro Moretti, Giuliano Panico, Fulvio Piccinini, and Andrea Wulzer. Anomalous Couplings in Double Higgs Production. *JHEP*, 08:154, 2012.

[17] Richard Phillips Feynman, Robert Benjamin Leighton, and Matthew Sands. *The Feynman lectures on physics; New millennium ed.* Basic Books, New York, NY, 2010. Originally published 1963-1965.

[18] Savas Dimopoulos, Stuart Raby, and Frank Wilczek. Proton decay in supersymmetric models. *Physics Letters B*, 112(2):133 – 136, 1982.

[19] David J Griffiths. *Introduction to elementary particles; 2nd rev. version*. Physics textbook. Wiley, New York, NY, 2008.

[20] M. Della Negra, P. Jenni, and T. S. Virdee. Journey in the search for the higgs boson: The atlas and cms experiments at the large hadron collider. *Science*, 338(6114):1560–1568, 2012.

[21] Jennifer Ouellette. Einstein's quest for a unified theory. *APS*, 2015.

[22] E A Davis and Isabel Falconer. *J.J. Thompson and the discovery of the electron*. Taylor and Francis, Hoboken, NJ, 2002.

[23] Oreste Piccioni. *The Discovery of the Muon*, pages 143–162. Springer US, Boston, MA, 1996.

[24] G. Danby, J-M. Gaillard, K. Goulianos, L. M. Lederman, N. Mistry, M. Schwartz, and J. Steinberger. Observation of high-energy neutrino reactions and the existence of two kinds of neutrinos. *Phys. Rev. Lett.*, 9:36–44, Jul 1962.

[25] M. L. Perl, G. S. Abrams, and et al Boyarski. Evidence for anomalous lepton production in $e^+ - e^-$ annihilation. *Phys. Rev. Lett.*, 35:1489–1492, Dec 1975.

[26] K. Kodama et al. Observation of tau neutrino interactions. *Phys. Lett.*, B504:218–224, 2001.

[27] S. M. Bilenky. Neutrino in Standard Model and beyond. *Phys. Part. Nucl.*, 46(4):475–496, 2015.

[28] S Chandrasekhar. *Newton's principia for the common reader*. Oxford Univ., Oxford, 2003. The book can be consulted by contacting: PH-AID: Wallet, Lionel.

[29] Hanoch Gutfreund and Jürgen Renn. *The road to relativity: the history and meaning of Einstein's "The foundation of general relativity" : featuring the original manuscript of Einstein's masterpiece*. Princeton University Press, Princeton, NJ, Apr 2015.

[30] J. Butterworth. *Smashing Physics*. Headline Publishing Group, 2014.

[31] W N Cottingham and D A Greenwood. *An Introduction to the Standard Model of Particle Physics; 2nd ed.* Cambridge Univ. Press, Cambridge, 2007.

[32] Eric W. Weisstein. Fundamental forces.

[33] Carl Bender. Mathematical physics.

[34] Andrew Wayne. QED and the Men Who Made It: Dyson, Feynman, Schwinger, and Tomonaga by Silvan S. Schweber. *The British Journal for the Philosophy of Science*, 46(4):624–627, 1995.

[35] C. Patrignani et al. Review of Particle Physics. *Chin. Phys.*, C40(10):100001, 2016.

[36] Michelangelo L Mangano. Introduction to QCD. (CERN-OPEN-2000-255), 1999.

[37] Matt Strassler. Of particular significance: Conversations about science with theoretical physicist matt strassler.

[38] S. L. Glashow. Partial Symmetries of Weak Interactions. *Nucl. Phys.*, 22:579–588, 1961.

[39] F. Englert and R. Brout. Broken symmetry and the mass of gauge vector mesons. *Phys. Rev. Lett.*, 13:321–323, Aug 1964.

[40] Peter W. Higgs. Broken symmetries and the masses of gauge bosons. *Phys. Rev. Lett.*, 13:508–509, Oct 1964.

[41] G. S. Guralnik, C. R. Hagen, and T. W. B. Kibble. Global conservation laws and massless particles. *Phys. Rev. Lett.*, 13:585–587, Nov 1964.

[42] Pauline Gagnon. *Who cares about particle physics? : making sense of the Higgs boson, the Large Hadron Collider and CERN*. Oxford University Press, 2016.